Available online at www.sciencedirect.com
SCIENCE DIRECT®
Acta Materialia 53 (2005) 3253–3260
Acta MATERIALIA
www.actamat-journals.com

Programmable nanoscale domain patterns in multilayers

Wei Lu *, David Salac

Department of Mechanical Engineering, University of Michigan, 2250 G.G. Brown Bldg. 2350 Hayward Street, Ann Arbor, MI 48109, USA

Received 28 January 2005; received in revised form 19 March 2005; accepted 24 March 2005

Abstract

The pattern formation in systems with multiple layers of adsorbate molecules is studied. We consider the presence of two types of molecules in each layer, which are characterized by different dipole moments. The patterns are characterized by the non-uniform distribution of the two molecules. A phase field model is developed to simulate the molecular motion and patterning under the combined actions of dipole moments, intermolecular forces, entropy and external electric field. The study reveals self-alignment, pattern conformation and the possibility to reduce the domain sizes via a layer by layer approach. It is also shown that the pattern in a layer may define the roadway for molecules to travel on top of. This, combined with electrodes embedded in the substrate, gives a great deal of flexibility to guide the molecular motion and patterning.

Keywords: Self-organization and patterning; Phase field models; Spinoidal decomposition; Nanostructure

1. Introduction

Self-organization is an efficient way to grow nanostructures with regular sizes and spacings on a substrate surface. As a representative system, the spontaneous domain pattern formation of adsorbate monolayers has attracted widespread interest [1–3]. Adsorbate molecules carry electric dipole moments, and the magnitude can be engineered by adding polar groups [4]. These molecules are mobile on a surface [5,6]. Domains coarsen to reduce the domain boundary energy and refine to reduce the electric dipole interaction energy. The competition determines the feature sizes and leads to stable patterns. A dipole type of interaction is characterized by a 1/distance^3 variation in the energy, which can be induced by electric, magnetic or elastic fields. Similar patterns and analogous mechanisms have been observed in diverse material systems, such as Langmuir films at the air–water interface [7,8], ferrofluids in magnetic fields [9,10], organic molecules on metal surfaces [11–13], and surface stress induced self-organization on elastic substrates [14,15].

An external field may be applied to direct the self-organization process. Molecular monolayers composed of electric dipoles can be manipulated with an electric field induced by an AFM tip, a ceiling above the layer, or an electrode array in the substrate [16–19]. The electric field also takes effect through dielectric inhomogeneity, which has been shown to cause domain patterns in dielectric films [20–22].

The mechanism of monolayer pattern formation gives insight into the study of analogous phenomena in multilayers, where pertinent experiments are lacking. Electrostatic interactions have been utilized to construct functional multilayer systems by the approach of electrostatic self-assembly (ESA) [23–25]. ESA processing involves dipping a chosen substrate into alternate aqueous solutions containing anionic and cationic molecules or nanoparticles, such as complexes of polymers, metal and oxide nanoclusters or proteins. This leads to alternating layers of polyanion and polycation monolayers.

* Corresponding author. Tel.: +1 734 647 7858; fax: +1 734 647 3170.
E-mail address: weilu@umich.edu (W. Lu).

1359-6454/$30.00
doi:10.1016/j.actamat.2005.03.029

Design of the precursor molecules and control of the sequence of the multiple molecular layers allow control over macroscopic electrical, optical, mechanical and other properties. While applications such as nanofiltration and photovoltaic devices have been demonstrated, the ESA process is generally limited to simple, laminar multilayer systems, with little or no lateral variation in the layer. We will show that for molecules carrying electric dipoles, dipole interaction can induce self-assembled patterns within each layer in a multilayer system. The capability is desirable for making complex structures, especially the formation of nanointerfaces and three dimensional nanocomposites.

Section 2 outlines a phase field model that describes the dynamic pattern formation process. Section 3 solves the electrostatic field in Fourier space. The numerical method to solve the diffusion equation is discussed in Section 4. Section 5 presents the numerical results. The simulations reveal self-alignment, pattern conformation and the possibility to reduce the domain sizes via a layer by layer approach. It is also shown that the pattern in a layer may define the roadway for molecules to travel on top of. This, combined with electrodes embedded in the substrate, gives a great deal of flexibility in guiding the molecular motion and patterning.

2. The phase field model

Phase field model has recently been used to study nanoscale surface phenomena. For instance, it has been applied to simulate the self-assembly of monolayers on a solid surface due to surface stress [26–31]. In this paper, we apply the approach to study multiple layers of molecules. We consider a domain size much larger than that of an individual molecule, such as tens of nanometers. Thus, a domain in each layer still contains many molecules and the continuum approach is applicable. The molecules evolve via a diffusion process. Fig. 1 shows a multilayer of molecules adsorbed onto a substrate. The first layer is in contact with the substrate, and the nth layer is the top layer. Each layer has a thickness of h_m, with m varying from 1 to n. The total thickness of the multilayer system is h_f. The space above the top layer can be either air or a dielectric fluid. The substrate surface coincides with the plane of $x_3 = 0$. An array of electrodes is embedded in the substrate at a depth of h_s. Each layer comprises two molecular species carrying different dipole moments. For the nth layer, let concentration C_n be the fraction of surface sites occupied by one of the two species, and regard it as a time-dependent, spatially continuous function, $C_n(x_1, x_2, t)$. The free energy of the top layer is given by

$$G = \int_A \left(g(C_n) + \beta |\nabla C_n|^2 + \frac{1}{2}\left(\frac{p_n}{h_n}\right)(\Delta\phi_n)_s \right) \mathrm{d}A + \int_A \left(\frac{p_n}{h_n}\right)(\Delta\phi_n)_e \, \mathrm{d}A. \quad (1)$$

The first integral is the 'self-energy' of the layer. The $g(C_n)$ term represents the chemical energy. We also lump any interface energy between the nth layer and its underlying layer into this term. To describe phase separation, we may prescribe $g(C_n)$ by any function with two wells. We assume a regular solution and the energy per unit area is given by

$$g(C_n) = \Lambda k_B T [C_n \ln C_n + (1 - C_n)\ln(1 - C_n) + \Omega C_n (1 - C_n)]. \quad (2)$$

The first two terms in the bracket result from the entropy of mixing, and the third term from the energy of mixing. Here, Λ is the number of surface sites per unit area, k_B the Boltzmann constant, T the absolute temperature, and Ω a dimensionless parameter measuring the bonding strength relative to the thermal energy. When $\Omega > 2$, the function $g(C_n)$ has double wells and the binary mixture separates into two phases. The second term in Eq. (1) is the phase boundary energy within the layer, with β being a material constant. These two terms are typical in the standard Cahn–Hilliard [32] model.

The third term in Eq. (1) describes the dipole assembly energy, i.e., the work to bring the dipole charges from infinity to the current configuration. Here, p_n is the dipole density per unit area of the top layer. We interpolate p_n linearly by the dipole densities of the two species, giving $p_n = \xi_n + \eta_n C_n$, where ξ_n and η_n are two material constants. The quantity $(\Delta\phi_n)_s$ is the potential jump across the nth layer thickness due to the dipole interaction within the layer. Note that $(\Delta\phi_n)_s$, and thus the assembly energy, is affected by the environment including the dielectric properties of the underlying layers and the substrate. The calculation of $(\Delta\phi_n)_s$ will be given in Section 3.

The second integral in Eq. (1) is the interactive energy of the top layer with the underlying layers and the

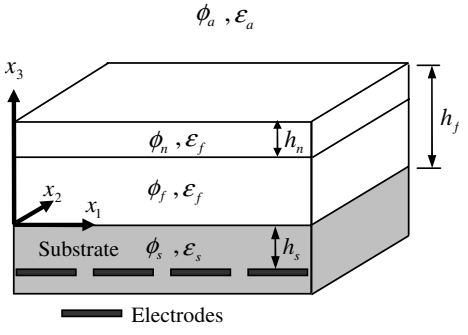

Fig. 1. Schematic of multiple layers of molecules absorbed onto a dielectric substrate. The substrate surface coincides with the plane of $x_3 = 0$. The top layer has a thickness of h_n. An array of electrodes is embedded at a distance of h_s from the substrate surface.

substrate. The dipoles in other layers and the applied field by the electrodes cause a potential difference, $(\Delta\phi_n)_e$, between the $x_3 = h_f$ and $x_3 = h_f - h_n$ surfaces in the dielectric media. The term $(p_n/h_n)(\Delta\phi_n)_e$ represents the energy of the top layer due to $(\Delta\phi_n)_e$. The factor of 1/2 marks the difference in the expressions of the dipole assembly energy, and the energy of dipoles in a given electric field.

The molecules in the top layer diffuse to reduce the energy given in Eq. (1). It is known that molecules at the surface have much higher mobility than those inside. Thus, when considering the diffusion of the top layer, we may assume that the buried layers do not diffuse. Following a procedure similar to [26,27], we obtain the diffusion driving force in the nth layer,

$$\mathbf{f} = -\frac{1}{\Lambda}\nabla\left(\frac{\partial g}{\partial C_n} - 2\beta\nabla^2 C_n + \eta_n\frac{(\Delta\phi_n)_s}{h_n} + \eta_n\frac{(\Delta\phi_n)_e}{h_n}\right). \tag{3}$$

A pattern reaches equilibrium when the driving force vanishes. Let $\mathbf{J}$ be the adsorbate flux. Assume that the flux is linearly proportional to the driving force, $\mathbf{J} = M\mathbf{f}$, where M is the mobility. The adsorbate conservation requires $\Lambda\partial C_n/\partial t = -\nabla\cdot\mathbf{J}$. These considerations together with Eq. (3) give the following diffusion equation:

$$\frac{\partial C_n}{\partial t} = \frac{M}{\Lambda^2}\nabla^2\left(\frac{\partial g}{\partial C_n} - 2\beta\nabla^2 C_n + \eta_n\frac{(\Delta\phi_n)_s}{h_n} + \eta_n\frac{(\Delta\phi_n)_e}{h_n}\right). \tag{4}$$

The last two terms in the bracket couple the evolution of the molecules to the electrostatic field. The calculation starts from the first layer. At a given time, the molecule distribution C_1 is known. The electrostatic field is determined by solving the boundary value problems. The resulting $(\Delta\phi_1)_s$ and $(\Delta\phi_1)_e$ are entered in the right-hand side of Eq. (4). The procedure is repeated for many time steps till the prescribed time. Then the calculation is started for the second layer, and so on. When considering the nth layer, the molecule distributions of C_m ($m = 1$ to $n-1$) are known from previous calculations. As will be evident, $(\Delta\phi_n)_s$ depends on C_n and $(\Delta\phi_n)_e$ depends on C_m ($m = 1$ to $n-1$).

3. Electrostatic field in Fourier space

This section solves the electrostatic field to obtain $(\Delta\phi_n)_s$ and $(\Delta\phi_n)_e$. First consider the calculation of $(\Delta\phi_n)_s$. The nth layer has an area dipole density of p_n. The dipole distribution is equivalent to a surface charge density of p_n/h_n at $x_3 = h_f$ and $-p_n/h_n$ at $x_3 = h_f - h_n$. The electric potential fields for the air, the nth layer, the underlying layers are denoted by ϕ_a, ϕ_n, ϕ_f and ϕ_s, respectively, as shown in Fig. 1. For simplicity, we assume that all the adsorbate layers have the same permittivity ε_f. The permittivities for the air and the substrate are ε_a and ε_s, respectively. The electric potential fields satisfy the Laplace equation in each region, namely

$$\nabla^2\phi_a = \nabla^2\phi_n = \nabla^2\phi_f = \nabla^2\phi_s = 0. \tag{5}$$

The potential fields are continuous at the boundary, giving

$$\begin{aligned}
&\phi_a(x_3 = h_f) = \phi_n(x_3 = h_f),\\
&\phi_n(x_3 = h_f - h_n) = \phi_f(x_3 = h_f - h_n),\\
&\phi_f(x_3 = 0) = \phi_s(x_3 = 0),\\
&\phi_s(x_3 = -h_s) = 0.
\end{aligned} \tag{6}$$

There is $\phi_s(x_3 = -h_s) = 0$ since we are considering the self-energy without any applied field. Gauss's law relates the electric displacement to the surface charge by

$$\begin{aligned}
&-\varepsilon_a\frac{\partial\phi_a}{\partial x_3}(x_3 = h_f) + \varepsilon_f\frac{\partial\phi_n}{\partial x_3}(x_3 = h_f) = \frac{p_n}{h_n},\\
&-\varepsilon_f\frac{\partial\phi_n}{\partial x_3}(x_3 = h_f - h_n) + \varepsilon_f\frac{\partial\phi_f}{\partial x_3}(x_3 = h_f - h_n) = -\frac{p_n}{h_n},\\
&-\varepsilon_f\frac{\partial\phi_f}{\partial x_3}(x_3 = 0) + \varepsilon_s\frac{\partial\phi_s}{\partial x_3}(x_3 = 0) = 0.
\end{aligned} \tag{7}$$

Equations (5)–(7) are solved analytically with Fourier transform to x_1 and x_2. For instance, $\hat{\phi}(k_1, k_2, x_3) = \int_{-\infty}^{\infty}\int_{-\infty}^{\infty}\phi(x_1, x_2, x_3)e^{-i(k_1x_1 + k_2x_2)}\,dx_1\,dx_2$, where k_1 and k_2 are the coordinates in Fourier space. The Laplace equations become ordinary differential equations $d^2\hat{\phi}/dx_3^2 = k^2\hat{\phi}$, where $k = \sqrt{k_1^2 + k_2^2}$. The solution takes the form of $\hat{\phi} = A\exp(kx_3) + B\exp(-kx_3)$. There is a pair of A and B for each of the ϕ_a, ϕ_n, ϕ_f and ϕ_s, and are determined by the boundary conditions (6) and (7). The solution gives

$$\frac{(\Delta\hat{\phi}_n)_s}{h_n} = -k\left(\frac{\eta_n\varepsilon_a}{\varepsilon_f^2}\right)W_k\hat{C}_n, \tag{8}$$

where

$$W_k = [\sinh(kh_f)\sinh(kh_s) + \cosh(kh_f)\cosh(kh_s)(\varepsilon_s/\varepsilon_f)]/D, \tag{9}$$

and

$$\begin{aligned}
D = {}&\sinh(kh_f)\left[\sinh(kh_s) + \cosh(kh_s)(\varepsilon_a\varepsilon_s/\varepsilon_f^2)\right]\\
&+ \cosh(kh_f)[\sinh(kh_s)(\varepsilon_a/\varepsilon_f) + \cosh(kh_s)(\varepsilon_s/\varepsilon_f)].
\end{aligned} \tag{10}$$

A similar approach solves the electrostatic field induced by the total $n-1$ layers of dipoles and the prescribed electrode potential of

$$\phi_s(x_1, x_2, -h_s) = U(x_1, x_2). \tag{11}$$

We obtain that

$$\frac{(\Delta\hat{\phi}_n)_e}{h_n} = -k\left(\frac{\eta_n\varepsilon_a}{\varepsilon_f^2}\right)R_k, \tag{12}$$

where

$$R_k = \frac{\hat{U}\varepsilon_s/\eta_n}{D} + \sum_{m=1}^{n-1}\left(\frac{\eta_m \hat{C}_m}{\eta_n}\right) \times \frac{\sinh(kz_m)\sinh(kh_s) + \cosh(kz_m)\cosh(kh_s)(\varepsilon_s/\varepsilon_f)}{D}, \tag{13}$$

and $z_m = \sum_{j=1}^{m} h_j$ is the distance between the upper surface of the mth layer and the substrate.

4. Numerical method

A comparison of the first two terms in Eq. (4) defines a length

$$b = \sqrt{\frac{\beta}{\Lambda k_B T}}. \tag{14}$$

In the Cahn–Hilliard model, this length scales the phase boundary thickness. A time scale is defined by

$$\tau = \frac{\beta}{M(k_B T)^2}. \tag{15}$$

Normalize the coordinates by b and the time by τ. A dimensionless number,

$$s_n = \frac{\varepsilon_a \eta_n^2}{\varepsilon_f^2 \sqrt{\beta \Lambda k_B T}}, \tag{16}$$

appears in the normalized equation. This number represents the strength of dipole interactions relative to the phase boundary energy, and affects the equilibrium domain size. The diffusion equation (4) in Fourier space is given by

$$\frac{\partial \hat{C}_n}{\partial t} = -k^2 \hat{P}_n - 2k^4 \hat{C}_n + k^3 s_n W_k \hat{C}_n + k^3 s_n R_k, \tag{17}$$

where $\hat{P}(k_1, k_2)$ is the Fourier transform of the function

$$P_n(x_1, x_2) = \ln\left(\frac{C_n}{1 - C_n}\right) + \Omega(1 - 2C_n). \tag{18}$$

We adopt an efficient semi-implicit method to integrate time in Eq. (17) [27,33]. For a given time t and time step Δt, denote $\hat{C}_n^t = \hat{C}_n(k_1, k_2, t)$, $\hat{P}_n^t = \hat{P}_n(k_1, k_2, t)$, and $\hat{C}_n^{t+\Delta t} = \hat{C}_n(k_1, k_2, t + \Delta t)$. Replacing $\partial \hat{C}_n/\partial t$ by $(\hat{C}_n^{t+\Delta t} - \hat{C}_n^t)/\Delta t$, $\hat{C}_n$ by $\hat{C}_n^{t+\Delta t}$, and $\hat{P}_n$ by $\hat{P}_n^t$ in Eq. (17) gives the time marching scheme. At each time step, the P_n^t field is calculated from the C_n^t field at every grid point according to Eq. (18). Both fields are transformed into $\hat{P}_n^t$ and $\hat{C}_n^t$ in Fourier space. Equation (17) gives $\hat{C}_n^{t+\Delta t}$. Then the inverse Fourier transform is applied to get $C_n^{t+\Delta t}$. The procedure is repeated till a prescribed time.

5. Simulation results

Equation (17) allows the simulation of an arbitrary number of layers, with the limiting factors being only computational power and time. The guiding effect of the electrodes and the underlying layer is of particular interest. With this consideration, we focus on two layers in this paper. Simulations are carried out with $256b \times 256b$ grids and periodic boundary conditions. The initial conditions are random. That is, the concentration has an average of $\bar{C}_n$ in the nth layer. The initial concentrations at the grid points fluctuate randomly within 0.001 from the average. The parameters used in all simulations are $\Omega = 2.2$, $\varepsilon_a/\varepsilon_s = \varepsilon_f/\varepsilon_s = 1$, $h_s/b = 10$, and $h_1/b = h_2/b = 0.5$. The parameters that vary in different simulations include the average concentrations $\bar{C}_1$, $\bar{C}_2$, the dimensionless parameters s_1, s_2, and the electrode voltage pattern $U(x_1,x_2)$. Three situations will be investigated: no applied electric field, an applied electric field to guide the first layer, and an applied electric field to guide both layers.

5.1. No applied electrical field

Figs. 2 and 3 show selected results for $U = 0$ and $s_1 = s_2 = 4$, darker color for higher concentration. The average concentration affects the pattern. It is not necessary to consider an average concentration greater than

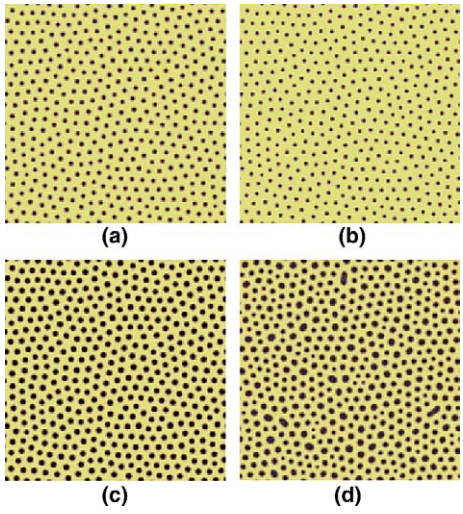

Fig. 2. Self-assembled domain patterns when $U = 0$: (a) shows the first layer pattern with $\bar{C}_1 = 0.3$, $t = 3000$. (b)–(d) show the second layer patterns at $t = 1000$ under various conditions; (b) The second layer pattern on top of (a) with $\bar{C}_2 = 0.2$. The positions of the dots are anchored by the first layer pattern. Note the domain size reduction; (c) The second layer pattern on (a) with $\bar{C}_2 = 0.4$. The dots are anchored at positions corresponding to those of the first layer; (d) The second layer pattern on a uniform first layer with $\bar{C}_2 = 0.4$. A uniform layer has no guiding effect. Note that the dots in (c) have much more uniform sizes than those in (d), suggesting an exciting possibility to increase the uniformity via a layer by layer approach.

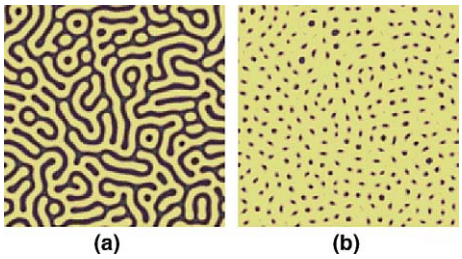

Fig. 3. Self-assembled domain patterns when $U = 0$: (a) shows the first layer pattern with $\bar{C}_1 = 0.5$, $t = 6000$; (b) shows the second layer pattern on top of (a) with $\bar{C}_2 = 0.2$, $t = 2000$. The dots arrange themselves to follow the underlying serpentine stripes.

0.5, since this can be easily accommodated by redefining the concentration with the other species.

Fig. 2(a) shows the pattern of the first layer at $t = 3000$. The average concentration is $\bar{C}_1 = 0.3$. The layer self-organizes into a triangle of dots. The dots have uniform size and form multiple grains. We have computed to $t = 10^6$, and the dots remain the same size. Without the dipole interaction, i.e., setting $s_1 = 0$, the simulation shows that the dots would have long coarsened into a single large dot. This confirms the refining effect of dipole interaction, which is necessary to stabilize the domain pattern.

Fig. 2(b)–(d) show the second layer patterns at $t = 1000$ under various conditions. Fig. 2(b) shows a second layer pattern, which has an average concentration of $\bar{C}_2 = 0.2$ and grows on top of the pattern in Fig. 2(a). We let the second layer evolve from a completely different random initial condition. The dots of the second layer stay at exactly the same positions as those in Fig. 2(a), suggesting an anchoring effect of the first layer. The dot size of the second layer is smaller due to the lower average concentration. Choosing a larger s_2 is another approach to reduce the domain size in the second layer. Equation (16) shows that a larger s_n indicates stronger dipole interaction and thus more refining.

Fig. 2(c) shows another situation. The second layer has an average concentration of $\bar{C}_2 = 0.4$, which is larger than that of the underlying layer. Similar correspondence between dot positions can be observed, though the second layer now has a larger domain size.

Fig. 2(d) shows what the second layer pattern looks like when there is no guidance of the first layer. The average concentration is $\bar{C}_2 = 0.4$, the same as that in Fig. 2(c). The simulation is performed by assigning a uniform concentration to the first layer. The magnitude of this concentration is insignificant since a uniform first layer has no contribution to the diffusion driving force of the second layer. The comparison between Fig. 2(c) and (d) clearly demonstrates the anchoring effect of the underlying layer. It is also interesting to observe that the dots in Fig. 2(c) have much more uniform sizes than those in Fig. 2(d). This suggests an exciting possibility of increasing the uniformity of self-organized domains via a layer by layer approach.

Fig. 3 shows a simulation with a different guiding pattern. The first layer has $\bar{C}_1 = 0.5$ and forms a serpentine stripe pattern shown in Fig. 3(a). The pattern difference between Fig. 3(a) and 2(a) indicates the effect of the average concentration. Fig. 3(b) shows the second layer pattern with $\bar{C}_2 = 0.2$. The dots arrange themselves to follow the underlying serpentine stripes, forming a pattern different from that in Fig. 2(b).

The observation of Figs. 2 and 3 suggests that the first layer pattern determines the ordering and lattice spacing, while the second layer determines the feature size. A scaling down of size can be achieved via multilayers. The interesting behavior suggests a potential fabrication method. In addition to self-assembly, the first layer pattern can be defined by embedded electrodes, proximal probe technique, or nanoimprinting.

5.2. An applied electric field to guide the first layer

In the following simulations, we apply voltage patterns by the electrodes to guide the first layer. Fig. 4(a) shows a voltage pattern composed of two dark stripes.

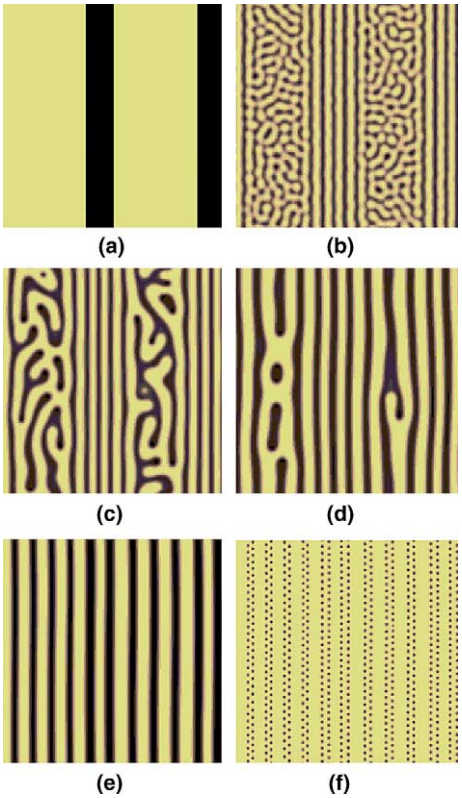

Fig. 4. (a) A voltage pattern. dark color: $U\varepsilon_s/\eta_1 = 0.1$, bright color: $U = 0$. (b)–(e) shows the evolution sequence of the first layer under the voltage guidance. $s_1 = 2$, $\bar{C}_1 = 0.5$. (b) $t = 100$. (c) $t = 1000$. (d) $t = 10^4$. (e) $t = 5 \times 10^4$. (f) The second layer pattern on top of (e) with $s_2 = 6$, $\bar{C}_2 = 0.2$, $t = 1000$.

The dark color corresponds to a voltage of $U\varepsilon_s/\eta_1 = 0.1$, and the bright color corresponds to $U = 0$. Fig. 4(b)–(e) show the evolution sequence of the first layer with $s_1 = 2$ and $\bar{C}_1 = 0.5$. The voltage guides the overall pattern of the monolayer without directly imposing the final configuration. In contrast to the serpentine stripe pattern in Fig. 3(a), an ordered parallel stripe pattern is obtained. Observe that concentration waves expand from the voltage stripes and form "seeds" of superlattices. These seeds grow into stripe colonies by consuming the nearby serpentine structures. After the first layer evolves to $t = 5 \times 10^4$, i.e., Fig. 4(e), we remove the external field, adsorb the second layer, and let it evolve. Fig. 4(f) shows the second layer pattern with $s_2 = 6$ and $\bar{C}_2 = 0.2$. The dots organize into nicely ordered parallel lines along the stripes in the first layer. The observation again confirms that the second layer pattern conforms to the first layer.

We next consider the guiding effect of a large applied voltage, and the effect of a first layer pattern with much larger feature sizes than those of the second layer. In the simulation we use a voltage pattern shown in Fig. 5(a), which comprises a stripe and two disks. The dark color region has a voltage of $U\varepsilon_s/\eta_1 = 10$. This magnitude is two orders larger than that in Fig. 4(a). The bright color region has $U = 0$. Fig. 5(b) shows the first layer pattern with $s_1 = 2$ and $\bar{C}_1 = 0.3$. The first layer replicates the voltage pattern. We have tried other average concentrations and obtained similar results. This suggests that a high voltage can completely sweep away any intrinsic patterns. We then remove the electric field and use the first layer to direct the second layer. With $s_2 = 6$ and $\bar{C}_2 = 0.3$, the second layer evolves into a pattern shown in Fig. 5(c). The dots form a triangular lattice and orientate to follow the edges of the first layer patterns. Compared to Figs. 4(e) or 2(a), the domain size of the guiding pattern in Fig. 5(b) is much larger. Fig. 5(c) shows that the guiding effect originates from the domain edges of the first layer, which we call the "seed sites". This is expected since a uniform first layer has not effect on the diffusion of the second layer. The seed sites gradually lose their influences on molecules farther away. The molecules such as those between the stripe and the disks feel an almost uniform underlying layer, and thus do not receive any direct guidance. However, they are influenced by the neighboring dots, which are further influenced by those even closer to the seed sites. This indirect way of guidance is analogous to crystal growth.

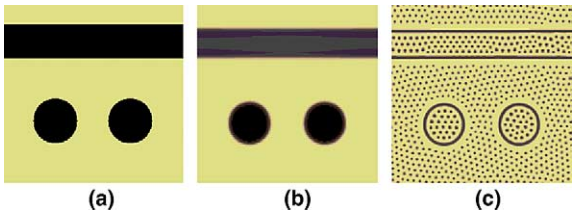

Fig. 5. (a) A voltage pattern. dark color: $U\varepsilon_s/\eta_1 = 10$, bright color: $U = 0$. (b) The first layer pattern with $s_1 = 2$, $\bar{C}_1 = 0.3$, $t = 2000$. (c) The second layer pattern with $s_2 = 6$, $\bar{C}_2 = 0.3$, $t = 1.5 \times 10^4$.

The simulations in Figs. 4 and 5 demonstrate the flexibility to use electrodes to construct a desired first layer. A second layer pattern can be engineered with the guidance of the first layer.

5.3. An applied electric field to guide both layers

It has been shown in the previous sections that the first layer has an anchoring effect on the second layer. This behavior is further exploited by applying a voltage pattern during the evolution of the second layer. Specifically, a particular voltage pattern is applied to construct the first layer. After that, we adsorb the second layer and apply a different voltage pattern. Different from the simulations in Figs. 4 and 5, the second layer is now under the guidance of both the first layer and an applied electric field. The study gives more insight into the potential application of multilayer systems.

We first apply a high voltage to obtain the first layer pattern shown in Fig. 6(a), which has $s_1 = 2$ and $\bar{C}_1 = 0.5$. The first layer consists of four vertical stripes, which replicates the voltage pattern. The voltage used is $U\varepsilon_s/\eta_1 = 10$. The second layer is then absorbed, which has $s_2 = 2$ and $\bar{C}_2 = 0.3$. The electrode is shifted to the right by a small amount relative to the first layer pattern. The new voltage pattern is shown in Fig. 6(b), with dark color corresponding to $U\varepsilon_s/\eta_2 = 1$. Fig. 6(c) shows the second layer pattern, which consists of four thin lines located at the overlapping regions of Fig. 6(a) and (b). The simulation suggests an exciting possibility to make well-controlled fine structures from coarse patterns. The structure size can be adjusted dynamically. The anchoring effect also indicates a possibility to construct a "roadway" to guide the motion of molecules on top of it, as shown in the following simulation.

Fig. 7(a) shows a monolayer roadway, which is obtained by applying a high voltage of $U\varepsilon_s/\eta_1 = 10$ at the electrodes. The layer replicates the voltage pattern and

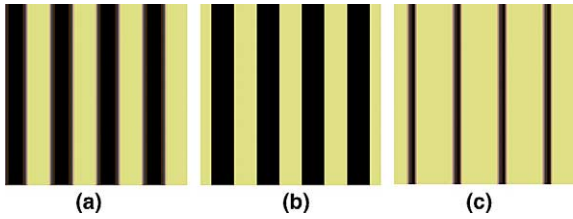

Fig. 6. (a) The first layer pattern with $s_1 = 2$, $\bar{C}_1 = 0.3$, $t = 1000$. The voltage used to obtain this pattern is $U\varepsilon_s/\eta_1 = 10$. (b) The new voltage pattern. dark color: $U\varepsilon_s/\eta_2 = 1$, bright color: $U = 0$. Note the shift of the voltage pattern relative to (a). (c) The second layer pattern under the guidance of both the first layer and the applied voltage. $s_2 = 2$, $\bar{C}_2 = 0.3$, $t = 1500$.

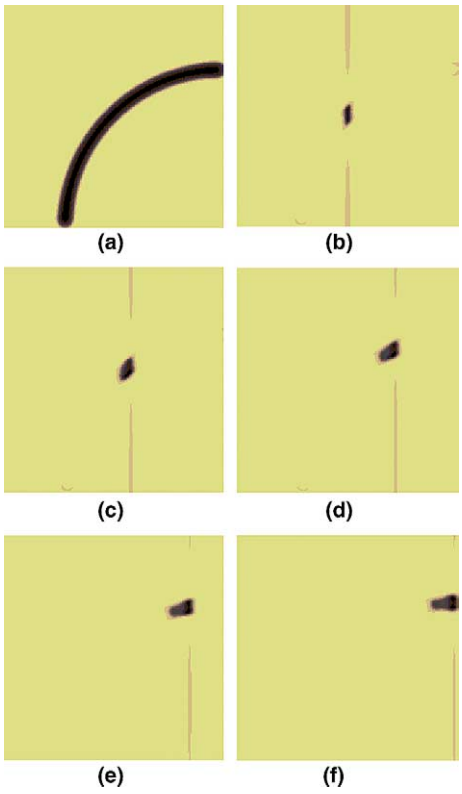

Fig. 7. (a) The first layer pattern with $s_1 = 2$, $\bar{C}_1 = 0.2$, $t = 5000$. The voltage used to obtain this pattern is $U\varepsilon_s/\eta_1 = 10$. (b)–(f) show a sequence of the second layer pattern guided by the first layer and a vertical voltage line with $U\varepsilon_s/\eta_2 = 5$. The line moves to the right at a speed of 0.016. $s_2 = 1$, $\bar{C}_2 = 0.2$. (b) $t = 800$. (c) $t = 2000$. (d) $t = 4000$. (e) $t = 6000$. (f) $t = 8000$.

has $s_1 = 2$ and $\bar{C}_1 = 0.2$. A second layer with $s_2 = 1$ and $\bar{C}_2 = 0.2$ is then absorbed on the first layer. The voltage pattern is set to be a straight vertical line centered in the computational cell. The line has a voltage of $U\varepsilon_s/\eta_2 = 5$. At $t = 800$ molecules accumulate at the intersection of the roadway and the voltage line, forming a dot shown in Fig. 7(b). We are going to move the dot and call it a molecular car [34]. Functional groups can be attached to the car, travel some distance and then be unloaded. We allow the voltage line to move to the right at a velocity of 0.016, which is normalized by b/τ. Fig. 7(b)–(f) show a sequence of the car's movement. Due to the anchoring effect of the first layer, the car follows the roadway and makes turns automatically. The car travels to the right at the same speed of the voltage line. The vertical movement is prescribed by the first layer pattern. The car changes its shape somewhat during the movement, but does not break apart. Because the car is only a small collection of molecules, the amount of materials moved can be very small. This could lead to exciting applications such as medical diagnostics, combinatorial chemistry and microfluidics. For instance, on a lab-on-a-chip it may be possible to transport different doses of chemicals from pools at the edges to the center of the chip, combine them into a new compound and test the effect. This process can be parallelized with many cars and multiple roadways. Tests of new drugs could thus be performed much more cheaply. Multilayer systems provide many possibilities and the flexibility to control the molecular motion.

6. Conclusion

Molecules absorbed onto a substrate are mobile and have electric dipoles. This paper studies the domain pattern formation of molecules in multilayer systems. A phase field model is developed to simulate the molecular motion and patterning under the combined actions of dipole moments, intermolecular forces, entropy, and external electric field. The guiding effect of the underlying layers and the voltage pattern are of particular interest. Taking a two-layer system as an example, we consider three situations in Section 5. The study reveals self-alignment, pattern conformation and the possibility to reduce the domain sizes via a layer by layer approach. It is also shown that the pattern in a layer may define the roadway for molecules to travel on top of. This combined with electrodes embedded in the substrate provides much flexibility. While the study focuses on two-layer systems, it is straightforward to consider more layers with Eq. (17). The overall picture should be similar. We look forward to experimental demonstrations of molecular assembly in multilayers.

Acknowledgment

The authors acknowledge financial support from National Science Foundation Career Award No. DMI-0348375.

References

[1] Bohringer M, Morgenstern K, Schneider W, Berndt R, Mauri F, De Vita A, et al. Phys Rev Lett 1999;83:324.
[2] Dmitriev A, Lin N, Weckesser J, Barth J, Kern K. J Phys Chem B 2002;106:6907.
[3] Xu F, Street S, Barnard J. J Phys Chem B 2003;107:12762.
[4] Evans SD, Urankar E, Ulman A, Ferris N. J Am Chem Soc 1991;113:4121.
[5] Kellogg GL. Surf Sci Rep 1994;21:1.
[6] Barth JV. Surf Sci Rep 2000;40:75.
[7] McConnell HM. Annu Rev Phys Chem 1991;42:171.
[8] Seul M, Andelman D. Science 1995;267:476.
[9] Dickstein AJ, Erramilli S, Goldstein RE, Jackson DP, Langer SA. Science 1993;261:1012.
[10] Richardi J, Ingert D, Pileni MP. Phys Rev E 2002;66:046306.
[11] Stranick SJ, Parikh AN, Tao YT, Allara DL, Weiss PS. J Phys Chem 1994;98:7636.
[12] Tamada K, Hara M, Sasabe H, Knoll W. Langmuir 1997;13:1558.

[13] Schneider K, Lu W, Owens T, Fosnacht D, Holl M, Orr B. Phys Rev Lett 2004;93.
[14] Ng KO, Vanderbilt D. Phys Rev B 1995;52:2177.
[15] Plass R, Last JA, Bartelt NC, Kellogg GL. Nature 2001;412:875.
[16] Heinrich A, Lutz C, Gupta J, Eigler D. Science 2002;298:1381.
[17] Gao Y, Suo Z. J Appl Phys 2003;93:4276.
[18] Rosei F, Schunack M, Naitoh Y, Jiang P, Gourdon A, Laegsgaard E, et al. Prog Surf Sci 2003;71:95.
[19] Suo Z, Gao Y, Scoles G. J Appl Mech 2004;71:24.
[20] Chou SY, Zhuang L. J Vac Sci Tech B 1999;17:3197.
[21] Schaffer E, Thurn-Albrecht T, Russell T, Steiner U. Nature 2000;403:874.
[22] Salac D, Lu W, Wang CW, Sastry AM. Appl Phys Lett 2004;85:1161.
[23] Iler RK. J Colloid Interf Sci 1966;21:569.
[24] Durstock MF, Spry RJ, Baur JW, Taylor BE, Chiang LY. J Appl Phys 2003;94:3253.
[25] Jin WQ, Toutianoush A, Tieke B. Langmuir 2003;19:2550.
[26] Suo Z, Lu W. J Mech Phys Solids 2000;48:211.
[27] Lu W, Suo Z. J Mech Phys Solids 2001;49:1937.
[28] Lu W, Suo Z. Phys Rev B 2002;65:205418.
[29] Lu W, Suo Z. Phys Rev B 2002;65:085401.
[30] Lu W, Kim D. Nano Lett 2004;4:313.
[31] Kim D, Lu W. Nanotechnology 2004;15:667.
[32] Cahn JW, Hilliard JE. J Chem Phys 1958;28:258.
[33] Chen L, Shen J. Comp Phys Commun 1998;108:147.
[34] Suo Z, Hong W. Proc Natl Acad Sci USA 2004;101:7874.